Spring 5-18-1959

The Absolute Excitation Functions for the I 127 (n,y) I 128 and Na 23 (n,y) and Na 24 Reactions

Richard L. Cubitt

ABSOLUTE EXCITATION FUNCTIONS - CUBITT

THE ABSOLUTE EXCITATION FUNCTIONS FOR THE $I^{127}(n,\gamma)I^{128}$ AND $Na^{23}(n,\gamma)Na^{24}$ REACTIONS

By

Richard L. Cubitt

A Thesis

Submitted in Partial Fulfillment of the

Requirements for the Degree of

Master of Science in Physics

The University of New Mexico

1958

This thesis, directed and approved by the candidate's committee, has been accepted by the Graduate Committee of the University of New Mexico in partial fulfillment of the requirements for the degree of

MASTER OF SCIENCE

E. H. Castetter
DEAN

May 18, 1959
DATE

Thesis committee

David Fromm
CHAIRMAN

Roy Thomas

Sam J. Bame, Jr.

ACKNOWLEDGEMENTS

The writer is indebted to the Los Alamos Scientific Laboratory of The University of California for making it possible to carry out this work. The writer also thanks Dr. D. K. Froman and Dr. S. J. Bame, Jr., for their advice and help in carrying out this experiment.

TABLE OF CONTENTS

LIST OF TABLES

LIST OF ILLUSTRATIONS

INTRODUCTION

Radiative capture (n,γ) cross sections, in addition to their theoretical interest, are of great practical importance to the technology of reactor design. A knowledge of the absolute excitation functions of the various materials employed in reactors permits calculation of the effect of these materials on the reactivity of a reactor, and also enables shielding calculations to be made.

Excitation functions are of interest theoretically because qualitative and quantitative information concerning the variation of energy level densities in nuclei may be obtained from such functions.

When a neutron is captured by a target nucleus, the resulting compound nucleus acquires an excitation energy equal to the kinetic energy of the neutron plus the binding energy of the neutron in the product nucleus. The compound nucleus can decay in a variety of ways depending upon its properties at this excitation energy.[1] For example, the excited compound nucleus can decay to its ground state by the emission of one or more gamma rays thus giving rise to the (n,γ) reaction. In some cases, the compound nucleus is stable in its ground state, but for some nuclei, radiative capture leads to an unstable product nucleus. In general, there are three physical features of (n,γ) reactions which permit the study of such reactions:

1) A neutron is "lost".

2) Capture gamma radiation is emitted.

3) A radioactive nucleus is produced.

---

[1] E. Segrè, Experimental Nuclear Physics, John Wiley and Sons (1953), II, pp. 321-325.

In this experiment, the third feature is employed to determine the absolute excitation functions for the reactions $Na^{23}(n,\gamma)Na^{24}$ and $I^{127}(n,\gamma)I^{128}$. The radioactive nucleus Na^{24} decays with a 15-hour half-life[2] in the manner shown in Fig. 1. I^{128} has a half-life of 25 minutes[2] and its decay scheme is shown in Fig. 2.

The absolute excitation function for $I^{127}(n,\gamma)I^{128}$ has been previously determined in the neutron energy range 15 kev to 2 Mev,[3] with a neutron energy spread of about 50 kev. A few isolated values of the absolute cross section for the $Na^{23}(n,\gamma)Na^{24}$ reaction have also been obtained.[3] The purpose of this experiment is twofold: (a) to determine the absolute excitation function for $I^{127}(n,\gamma)I^{128}$ with better accuracy and energy resolution than in previous experiments, and (b) to obtain an absolute excitation function for $Na^{23}(n,\gamma)Na^{24}$.

EXPERIMENTAL PROCEDURES FOR THE MEASUREMENT OF ABSOLUTE EXCITATION FUNCTIONS

Na^{24} and I^{128} activities were produced by irradiating NaI(Tl) crystals with monoenergetic neutrons from the $T(p,n)He^3$ and $Li^7(p,n)Be^7$ reactions. The crystals, after irradiation, were placed in a mineral oil well on top of a photomultiplier tube. The pulses from the photomultiplier tube were then fed into an amplifier and from the amplifier into a multichannel analyzer.

The decay scheme for Na^{24} (Fig. 1) shows that a beta particle is emitted for each decay of a Na^{24} nucleus. Thus, a decay of a Na^{24} nucleus will result in a pulse from the photomultiplier tube. I^{128} decays

---

[2] J. Hollander, I. Perlman, and G. Seaborg, Rev. Mod. Phys. 25, 469 (1953); also N. Benczer and others, Phys. Rev. 101, 1027 (1956).

[3] D. Hughes and R. Schwartz, Neutron Cross Sections, Brookhaven National Laboratory (1957) Supplement I to BNL 325.

Fig. 1 - The decay scheme of Na^{24}.

Fig. 2 - The decay scheme of I^{128}.

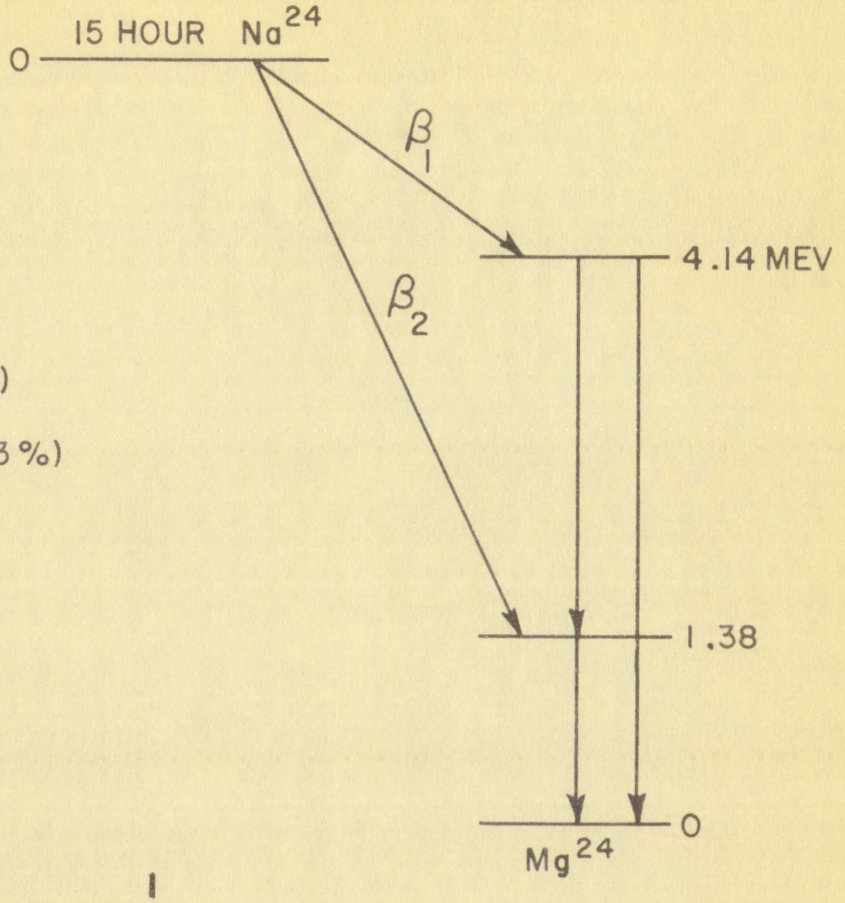

β_1 = 1.4 MEV (~100%)

β_2 = 4.17 MEV (~0.003%)

1

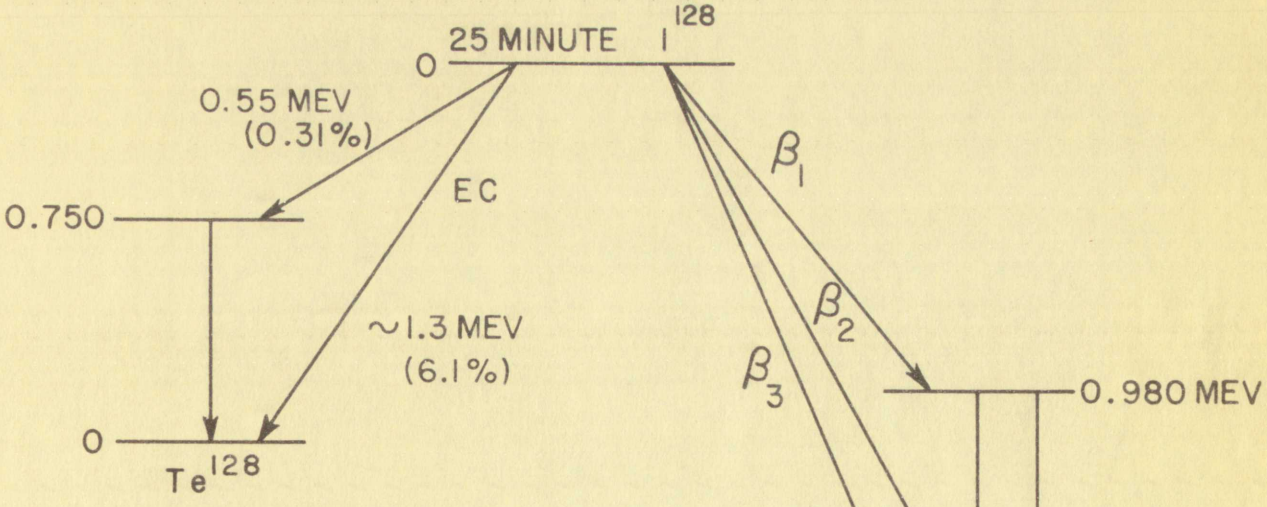

β_1 = 1.125 MEV (2%)

β_2 = 1.665 MEV (15.5%)

β_3 = 2.120 MEV (76.0%)

2

by beta particle emission 94% of the time and by electron capture 6% of the time (Fig. 2).[2] Electron capture by I^{128} results in the production of Te^{128} x-rays with 26 kev energy. A NaI crystal is almost 100% efficient in detecting these low-energy x-rays so a decay of an I^{128} nucleus to Te^{128} will also result in a pulse from the photomultiplier tube. Thus, the crystals serve not only as targets but also as nearly 100% efficient detectors. The large difference in the half lives of the sodium and iodine activities made it possible to resolve them quite well.

The absolute cross sections were computed from a knowledge of the absolute neutron fluxes, the activities of the crystals, the weights of the crystals, and the source-crystal geometries. The procedures by which the absolute excitation functions were obtained are described in detail below.

Neutron Sources

Monoenergetic neutron fluxes were produced by the use of the $Li^7(p,n)Be^7$ and $T(p,n)He^3$ reactions with the Los Alamos 2.5-Mev electrostatic accelerator which provided a magnetically separated proton beam. The accelerator was controlled at the proper voltage by passing the diatomic beam through an electrostatic analyzer which was calibtated with the $Li^7(p,n)Be^7$ neutron threshold.

The $Li^7(p,n)Be^7$ reaction[4] has a threshold energy of 1.883 Mev and may be used to produce monoenergetic neutrons in either of two ways. The energy of the neutrons emerging at a given angle with respect to the incident proton beam can be varied by changing the proton energy, or the proton energy can be held at a fixed value and neutrons of various energies emerge at various angles. With the accelerating voltage obtainable, the combination

---

[4] R. F. Taschek and A. Hemmendinger, Phys. Rev. 74, 373 (1948); A. Langsdorf, J. Monahan and W. A. Reardon, A Tabulation of Neutron Energies from Monoergic Protons on Lithium, Argonne National Laboratory, 5219 (1954).

of the two methods provides a neutron energy range from about 5 kev to 500 kev. Figure 3 shows the energy of the neutrons at 0^{o} as a function of the incident proton beam energy. The variation of neutron energy with angle for a few typical proton energies is shown in Fig. 4. For proton energies up to about 40 kev above threshold, the neutrons are double valued in energy at each angle in the forward direction; this effect is due to the center-of-mass velocity. For proton energies greater than 2.3 Mev the neutrons are double valued in energy due to the excitation of the 430 kev level in Be^{7}.

Lithium targets were made by evaporating normal lithium from an electrically heated furnace onto a 10 mil thick tantalum disc on the end of a target assembly. In order to place large proton beams (30-40 μa) on the target without heating the tantalum disc to temperatures which would cause evaporation of the lithium, the above assembly was gyrated so that the proton beam traced a 1-inch diameter circle on the lithium layer. Also, the proton beam was electrically rotated in a 1/8-inch diameter circle and an air-water spray was used to cool the target backing. Proton beams as high as 60 μa have been placed on these targets for a few hours with no observable loss of lithium.

The thickness of the lithium layer must be determined in order to calculate the neutron energy spread from the source because there is degradation in energy of the proton beam passing through the target. The neutron energy spread for each irradiation was the difference in energy between neutrons produced at the front of the lithium layer and the neutrons produced at the back of the layer. The energy of the neutrons produced at the center of the layer was taken to be the mean energy of the neutrons for the irradiation. Target thicknesses were measured by observing the neutron

Fig. 3 - Neutron energy at 0° as a function of proton energy - $Li^{7}(p,n)Be^{7}$ Reaction.

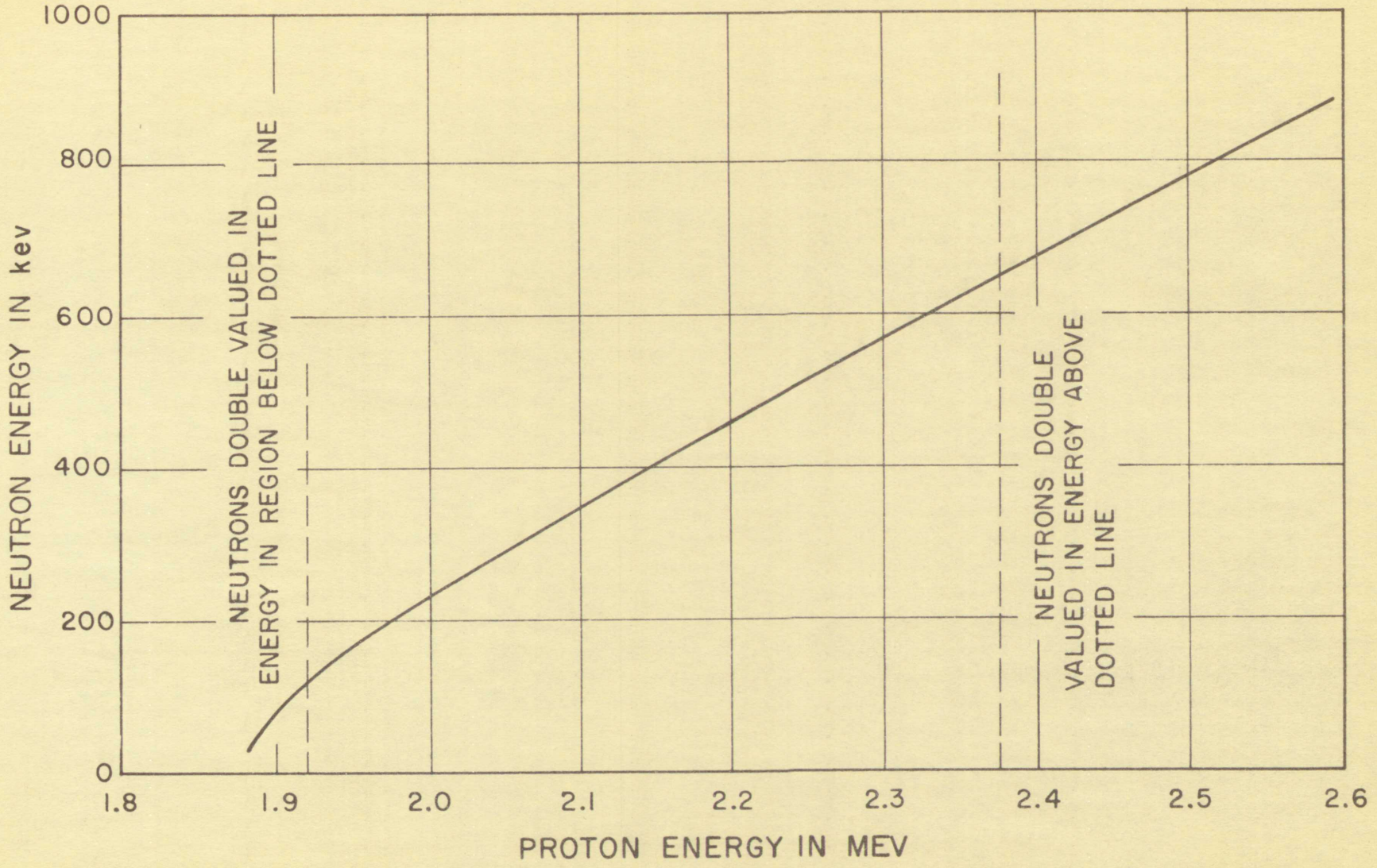
NEUTRON ENERGY IN kev
1000
800
600
400
200
0
1.8
1.9
2.0
2.1
2.2
2.3
2.4
2.5
2.6
PROTON ENERGY IN MEV
NEUTRONS DOUBLE VALUED IN ENERGY IN REGION BELOW DOTTED LINE
NEUTRONS DOUBLE VALUED IN ENERGY ABOVE DOTTED LINE

Fig. 4 - Angular dependence of neutron energy - $Li^7(p,n)Be^7$ reaction.

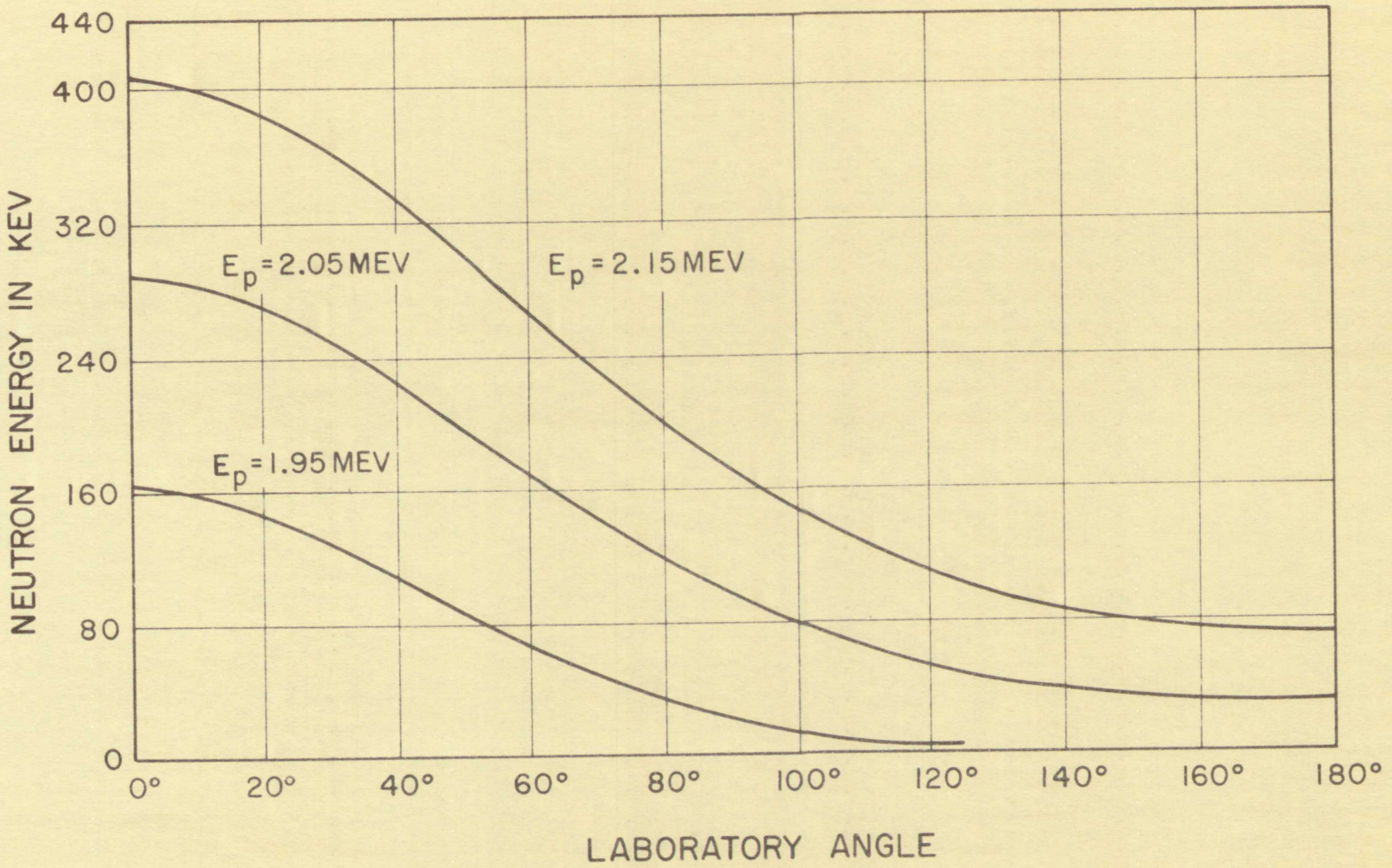
NEUTRON ENERGY IN KEV
440
400
320
240
160
80
0
E_p = 2.05 MEV
E_p = 2.15 MEV
E_p = 1.95 MEV
0°
20°
40°
60°
80°
100°
120°
140°
160°
180°
LABORATORY ANGLE

yield at 0° with a flat response long counter[5] as a function of proton bombarding energy. Because of the center-of-mass velocity, the neutrons will emerge in a narrow cone in the forward direction at the threshold energy. With a very thin target, the maximum of the neutron yield would be at the threshold energy. As the proton energy is increased, the yield rapidly decreases as the cone opens up but does not decrease to zero. For a thick target the neutron yield increases with proton energy until the protons at the back of the target have threshold energy and subsequently decreases. During the experiment, the target thickness was determined by the difference between the proton bombarding energy at threshold and at the maximum of the neutron yield. With large proton beams placed on a target for a few hours, it was observed that a visible layer of carbon was formed. The threshold energy for the target was therefore measured periodically to insure that no unreasonable amount of carbon had deposited on the lithium layer.

Neutrons above 400 kev were produced by passing protons through a tritium gas target to produce the reaction $T(p,n)He^3$.[6] This reaction has a Q-value of -764 kev, so that with the obtainable accelerating voltages, it can be used to provide a neutron energy range from 0.3 to 1 Mev. Figure 5 shows the energy of the neutrons at 0° as a function of proton energy.

The tritium gas was confined to the target volume by the use of a thin aluminum foil which was cooled indirectly by an air spray. The target length was about 3 cm and the target was usually filled to about 30-60 cm Hg pressure. The mean energy loss of the protons in passing through the foil and gas was calculated from range-energy data.

---

[5] A. O. Hanson and J. L. McKibben, Phys. Rev. 72, 673 (1947).

[6] G. Jarvis and others, Phys. Rev. 79, 929 (1950); J. Marion and B. Allen, A Tabulation of Neutron Energies from Various Charged Particle Reactions, Shell Development Company, (1955).

Fig. 5 - Neutron energy at 0^{o} as a function of proton energy - $T(p,n)He^{3}$ reaction.

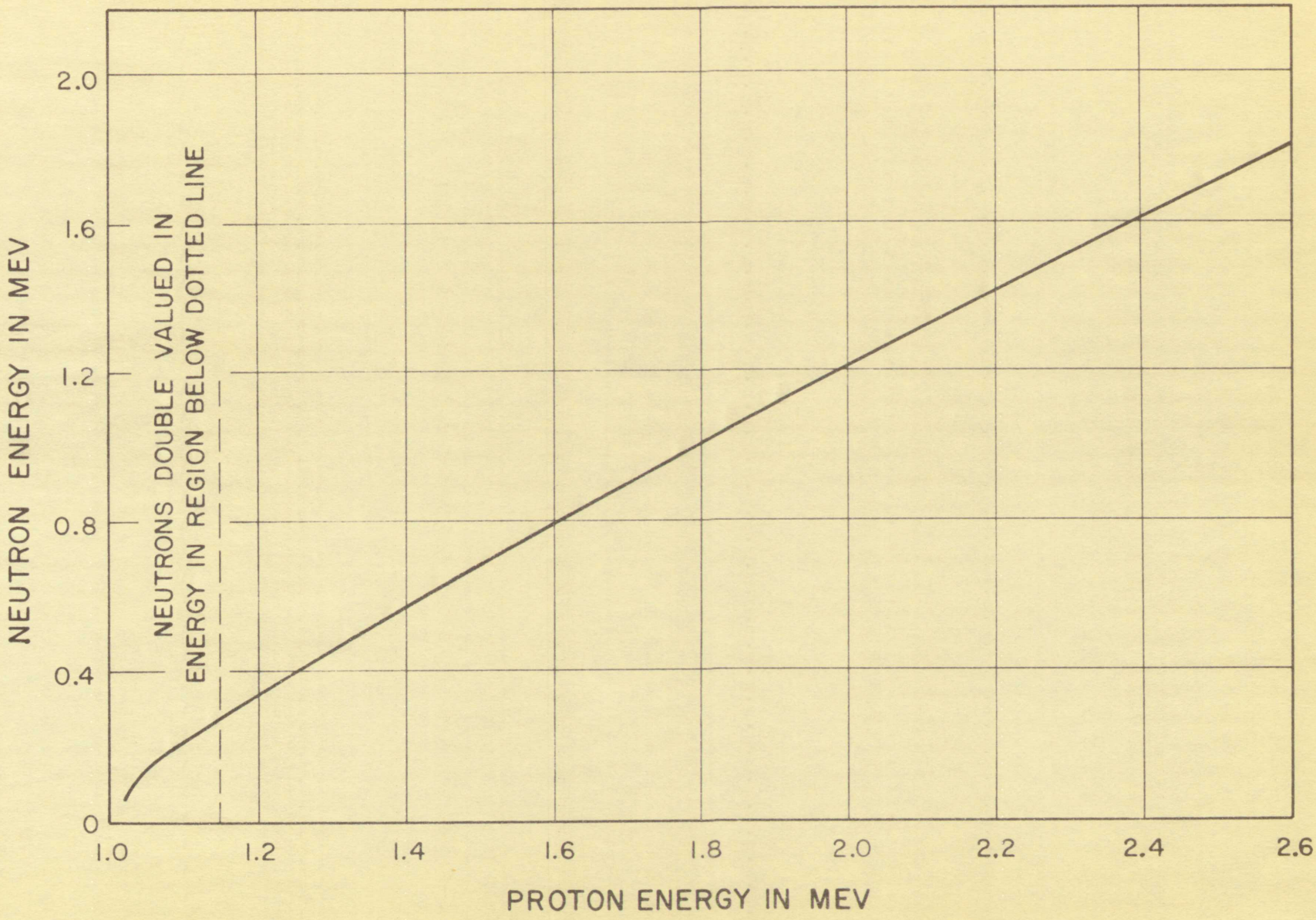
NEUTRON ENERGY IN MEV
2.0
1.6
1.2
0.8
0.4
0
NEUTRONS DOUBLE VALUED IN
ENERGY IN REGION BELOW DOTTED LINE
1.0
1.2
1.4
1.6
1.8
2.0
2.2
2.4
2.6
PROTON ENERGY IN MEV

The energy straggling of the proton beam in passing through the non-uniform aluminum foil limited the energy resolution which could be obtained with this reaction. The straggling effect was determined by filling the target to a few cm of Hg-pressure and observing the neutron yield at 0° as a function of proton energy with a flat response long counter. In the absence of a foil, a sharp peak would occur at the threshold energy of the reaction. However, with the foil, the width of the peak is increased by the straggling of the proton beam. The half-width at half-maximum of the resulting peak was used as the value for the straggling in determining the neutron energy spread of the irradiations. The half-width energy spread due to straggling in the foil was about 26 kev.

Also, there is a spread in neutron energy caused by the degradation in energy of the proton beam in passing through the gas because the neutrons are produced throughout the length of the gas target. This energy spread is the difference in energy between neutrons produced at the front of the gas and the neutrons produced at the back of the gas. The total energy spread is the sum of the energy spread due to the gas and the full-width spread (52 kev) due to straggling in the foil. The energy of the neutrons produced in the center of the gas target was taken to be the mean energy of the neutrons for the irradiation.

Measurement of Absolute Neutron Flux

Many experimental techniques have been developed to measure absolute neutron fluxes.[7] Perhaps the most accurate of these methods is the recoil particle method employing hydrogen as a source of recoiling protons since the n-p scattering cross section has been very well measured. However, the

[7] J. L. Fowler and J. E. Brolley, Phys. Rev. 28, 103 (1956).

use of the recoil particle method requires a very precise counter design and a complete understanding of the various wall and edge effects in the counter. A somewhat less accurate method of determining absolute neutron fluxes is the method of secondary standards. This method is generally less complicated since it makes use of neutron reaction cross sections which have been determined by methods like the recoil particle method. In this experiment a fission detector was employed as a secondary standard in measuring the absolute neutron flux, since the U^{235} fission cross section has been accurately determined in the neutron energy range 20 kev to about 10 Mev by comparison with the hydrogen scattering cross section.[8]

The fission detector was internally constructed of two parallel platinum discs, 0.005 inch thick and 0.368 inch apart. One plate contained 507.5 μg of U^{235} very uniformly deposited on a circular area 1.032 inches in diameter. The plates were housed in a thin-walled stainless steel cylinder which was sealed at one end by a stainless steel hemispherical cap. During flux measurements, the hemispherical cap faced the neutron source. The wall thicknesses were made thin, of the order of 0.010-0.015 inch to reduce the amount of scattering material as much as possible. The fission detector was covered with 0.016 inch thick cadmium sheet to eliminate counts from the background thermal neutron flux. Pulses from the detector were fed into an amplifier and from the amplifier were displayed on a multichannel analyzer. Very good resolution between the pulse sizes produced by the α particles and fission events was obtained since the U^{235} deposit was very thin and the plates were quite far apart. Fig. 6 shows a pulse height distribution obtained from this counter. The integrated number of pulses

---

[8] D. W. Allen and R. L. Henkel, Progress in Nuclear Engineering (Pergamon Press), Series I, II (in press).

Fig. 6 - Pulse height distribution from fission detector.

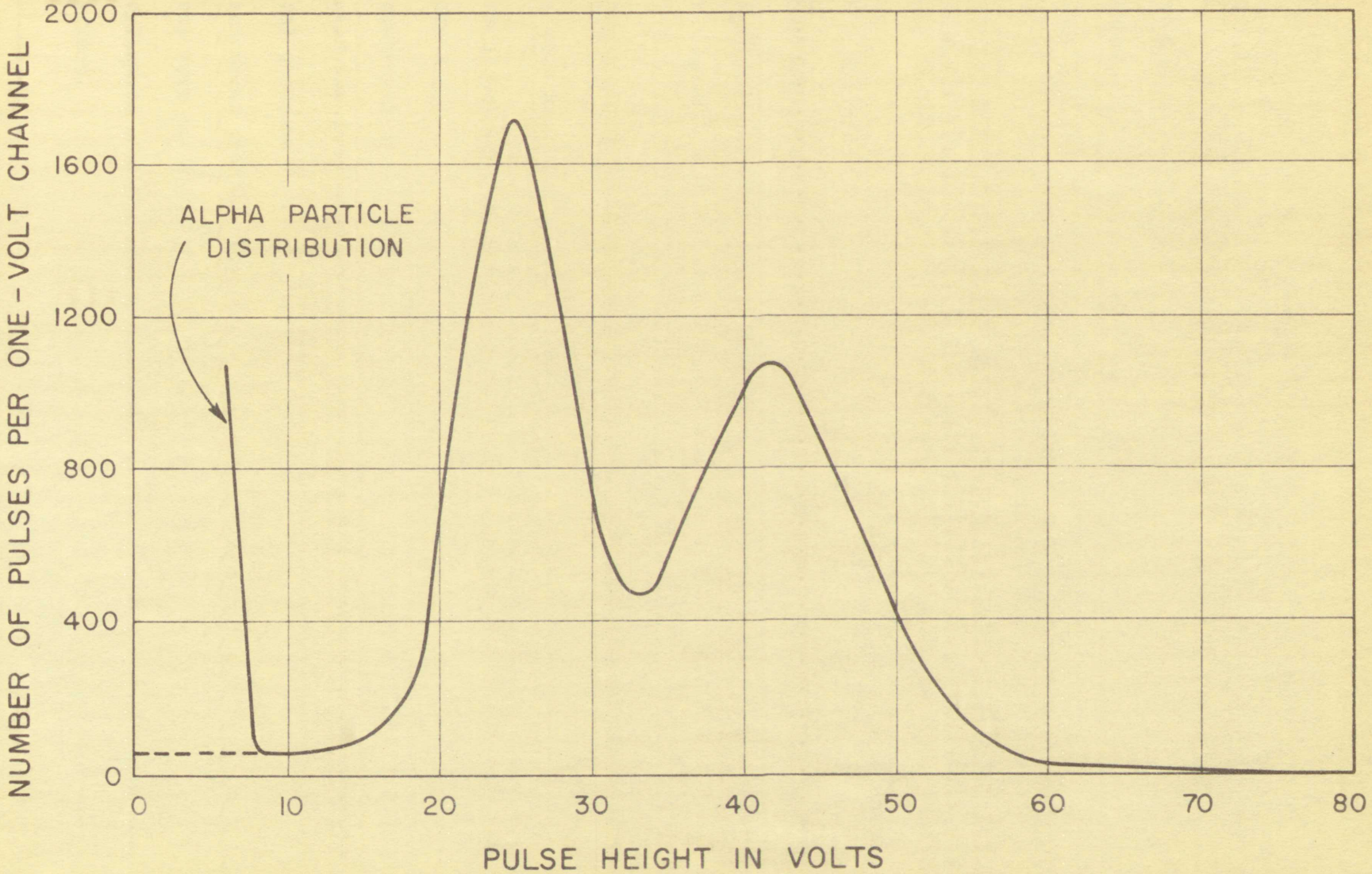
NUMBER OF PULSES PER ONE-VOLT CHANNEL
2000
1600
1200
800
400
0
ALPHA PARTICLE
DISTRIBUTION
0
10
20
30
40
50
60
70
80
PULSE HEIGHT IN VOLTS

was found by extrapolating the fission distribution to zero pulse height. A probable error of ± 2% was assigned to the number because of the uncertainty in this extrapolation.

The absolute neutron flux was calculated from a knowledge of the number of U^{235} atoms in the layer, the number of fission events and the absolute fission cross section of U^{235}. The expression used for calculating the flux was:

$$F(\theta,E_n) = C/N\Omega\sigma_f(E_n)$$

$F(\theta,E_n)$ = the number of neutrons of energy E_n per unit solid angle at the angle θ.

C = number of counts in the fission pulse height distribution.

Ω = solid angle subtended by the fission layer from the source at the angle θ.

$\sigma_f(E_n)$ = the U^{235} fission cross section at the neutron energy E_n.

N = number of U^{235} atoms per cm^2 in the layer.

The error in the measurement of neutron fluxes resulting from the scattering of neutrons by the detector's walls, was estimated to be about ± 2%. For a parallel flux of neutrons incident on a spherical shell, with a small detector placed at the center of the shell, the number of neutrons scattered out of the detector by the shell is compensated for by those scattered into the detector by the shell.[9] The hemispherical cap and cylinder used for the fission detector form a first order approximation to the spherical geometry case. Approximate calculations showed that the number of neutrons scattered out of the fission foil by the central part of the hemispherical cap were compensated by those scattered in by the rest of the cap and the cylinder. An error of ± 2% was assigned to flux measurements due to this effect.

---

[9] H. A. Bethe, J. R. Beyster and R. E. Carter, Journal of Nuclear Energy, 4, 3 (1957).

The error in flux measurements, resulting from the uncertainty in the U^{235} fission cross section, was estimated to be ± 5% for neutrons with energies above 150 kev, ± 10% for neutrons with energies between 60 kev and 150 kev, and ± 30% for neutrons with energies below 60 kev.

Irradiation and Counting Procedure for Obtaining I^{128} Activity.

NaI crystals in the form of cylinders, 2 cm in diameter and 0.5 cm thick were mounted with the crystal axes pointing toward the neutron source and were then irradiated with neutrons to produce the reaction $I^{127}(n,\gamma)I^{128}$. Figure 7 shows the pulse height distribution obtained from a crystal irradiated for about 5 minutes. The peak at 1.5 volts is due to the Te^{128} K x-rays associated with e^- capture by the I^{128} nuclei. The activity decayed with a clean 25 minute half-life indicating that a negligible amount of Na^{24} activity was produced during the short irradiation time.

Because NaI is hygroscopic, the crystals were protected from the atmosphere by storing them in mineral oil. The crystals were weighed on a microbalance after carefully wiping the mineral oil from the crystal. The time required to weigh each crystal was short enough so that no visible decomposition of the crystal occurred during the weighing. During the irradiation the crystals were protected by placing them in thin rubber fingers cut from surgical type gloves. The crystals were then placed on thin brass discs soldered to the ends of steel rods. The steel rods were held by a light aluminum ring which allowed the crystals to be positioned at accurately known angles and distances from the neutron source. Neutrons with energies of 20 to 500 kev were produced by the $Li^7(p,n)Be^7$ reaction and neutrons with energies above 500 kev were produced by the $T(p,n)He^3$ reaction. Nearly all of the irradiations were made at 0° with respect to the incident proton beam

Fig. 7 - Pulse height distribution of I^{128} activity.

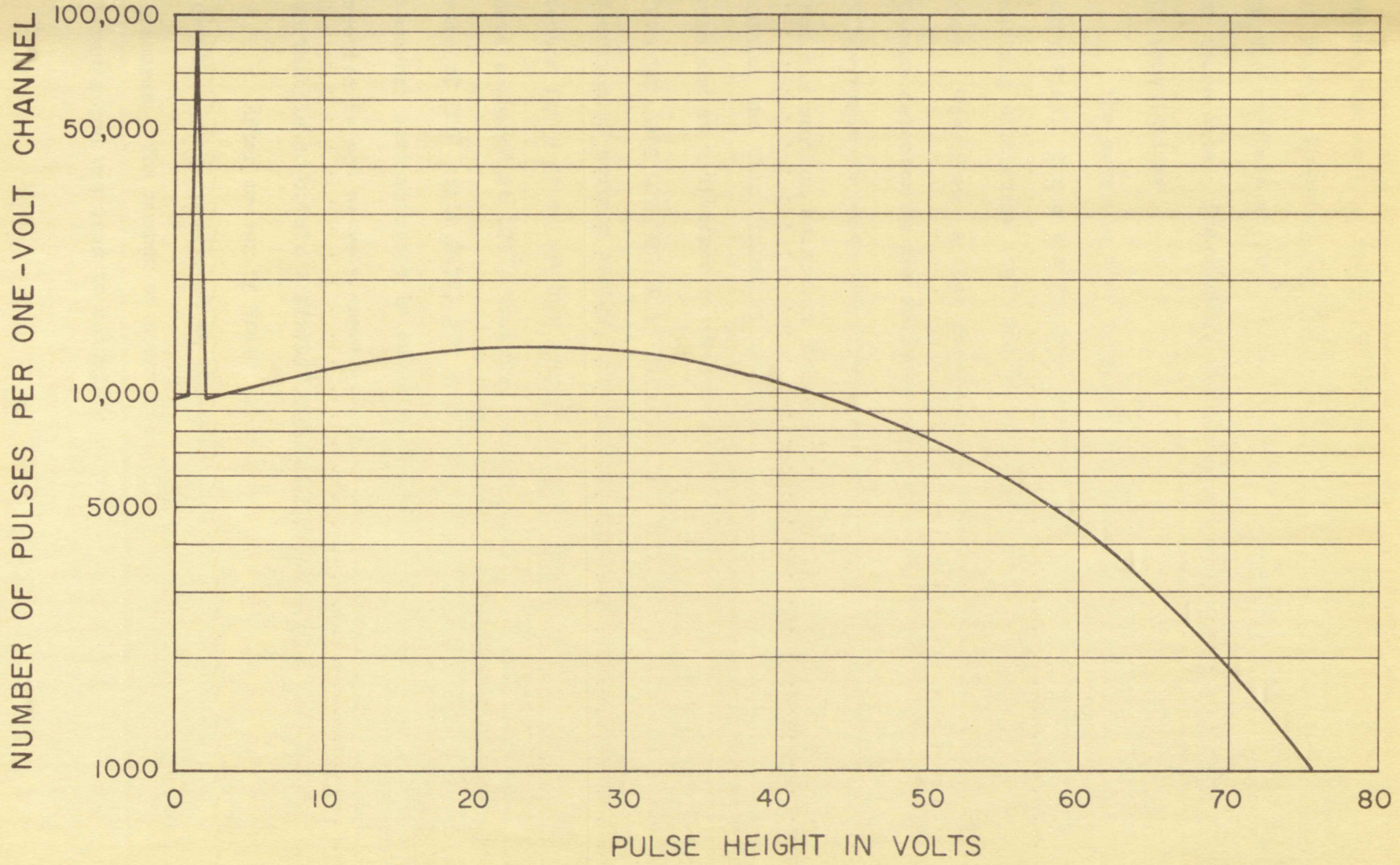
NUMBER OF PULSES PER ONE-VOLT CHANNEL
100,000
50,000
10,000
5000
1000
0
10
20
30
40
50
60
70
80
PULSE HEIGHT IN VOLTS

because the neutron energy spread for a given yield of neutrons is a minimun there. However, for the data below 130 kev it was necessary to irradiate the crystals at 120°, thus resulting in somewhat poorer energy resolution for those data. The crystal-to-neutron source distance was about 10 cm for all irradiations.

The crystals were irradiated for about 90 seconds to obtain reasonable activities. Since the fission detector was very inefficient, reasonable counting statistics could not be obtained from it during such short irradiation times. Therefore, a flat response long counter was calibrated against the fission detector in the following manner: the fission detector was placed at the angle at which the crystal was to be irradiated and the distance from the neutron source to the detector was accurately measured. The long counter was then placed at an angle of about 60° with respect to the proton beam and at a distance of about eleven feet from the source. Ratios of counts from the long counter to counts from the fission detector were found as a function of neutron energy. The number of counts taken in the fission detector for a given neutron energy was never less than 1000, except for the data obtained at 120°, thus the counting statistics were about 3%. In the case of 120° angle data, 600 counts were taken in the fission detector giving somewhat less accuracy in counting statistics. However, the fission cross section is not as well known in this low energy range and it did not seem worthwhile to obtain a greater number of counts.

After measuring these ratios, the fission detector was removed and crystals were irradiated at the same energies at which the ratios were measured. The number of counts from the long counter obtained during an irradiation was used to calculate the absolute neutron flux. The number of

neutrons scattered into the long counter by the fission detector, to a first order approximation, is compensated by the number of neutrons that are scattered into the long counter by the sample ring and crystal. However, an error of ± 2% has been assigned to the measurement to cover this difference in scattering effect.

After the irradiation the crystal was placed in a mineral oil well on the top of a DuMont 6292 photomultiplier tube and the number of pulses obtained in a multichannel analyzer in a 5 minute interval was observed. Figure 8 shows a block diagram of the detecting system. Pulses from the photomultiplier tube were fed to a preamplifier and amplifier and then into the input of a 10-channel pulse-height analyzer. The gain of the system was such that the peak from the Te^{128} x-ray appeared in the lower channels. All pulses too large to be seen by the 10th channel of the analyzer were recorded in a surplus channel. The integrated number of pulses was obtained by extrapolating the pulse height distribution to zero pulse height. A ± 2% error was assigned to this number because of the uncertainty in the extrapolation.

The data in the neutron energy range 150 to 500 kev were obtained with a twelve kev thick Li target. A 20 kev thick Li target was used for the irradiations at 120°.

Irradiation and Counting Procedures for Obtaining Na^{24} Activity

The procedures for obtaining Na^{24} activity were almost identical to those for obtaining the I^{128} activity. However, to obtain reasonable Na^{24} activities, so that the counting statistics did not limit the accuracy of the results, much longer irradiation times were needed. Also, higher yield neutron sources were used, resulting in poorer neutron energy resolution than was obtained for the iodine activations. The necessity for longer

Fig. 8 - Block diagram of the detecting system.

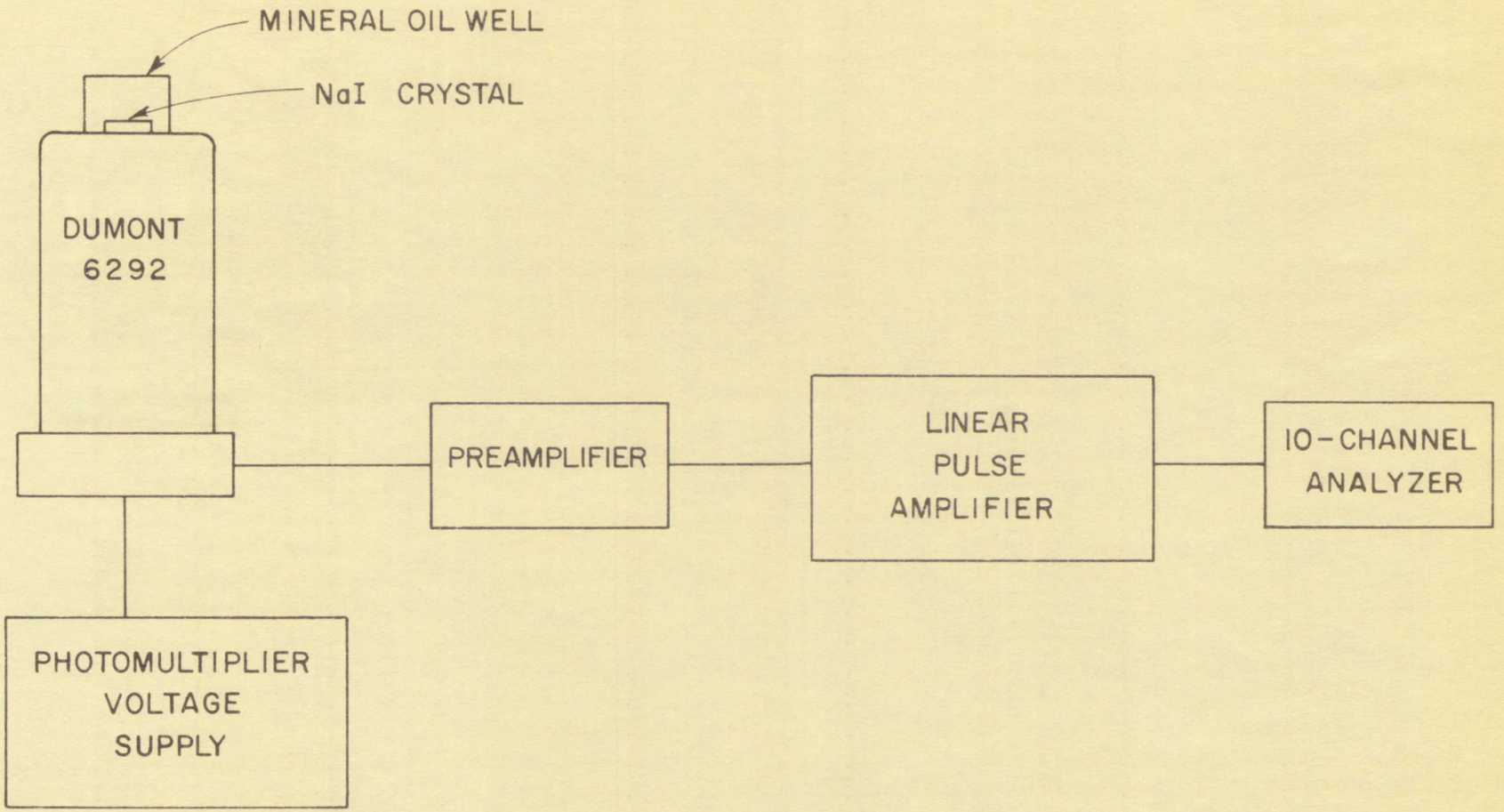
MINERAL OIL WELL
NaI CRYSTAL
DUMONT
6292
PREAMPLIFIER
LINEAR
PULSE
AMPLIFIER
10-CHANNEL
ANALYZER
PHOTOMULTIPLIER
VOLTAGE
SUPPLY

irradiation times and more prolific neutron sources resulted from the smaller (n,γ) cross section of Na^{23} and the longer half-life of Na^{24} as compared with the iodine case. Figure 9 shows a pulse height distribution obtained from a crystal about 10 hours after a very intense irradiation. The absence of the Te^{128} x-ray peak shows that a negligible amount of I^{128} activity was present. The activity decayed with a clean 15-hour half-life.

The data in the neutron energy range 175 to 500 kev were obtained at 0° using a 68 kev thick Li target. The neutron energy range below 180 kev was covered by placing six crystals at various angles around a 40 kev thick lithium target and irradiating them simultaneously for 11 hours. Data above 500 kev were obtained by making irradiations at 0° with the $T(p,n)He^3$ source. After waiting for the I^{128} activity to decay, the crystals were counted in the same detector system as used for I^{128}.

The gain of the detecting system was such that nearly all of the pulses were displayed in the surplus channel of the 10 channel analyzer. The total number of counts was then determined by extrapolating the pulse height distribution to zero pulse height. The crystals were counted for a length of time such as to obtain about 1% counting statistics. Since the counting rates of the samples were fairly small, varying from about 200-600 counts/minute, it was necessary to subtract a background counting rate of about 20 counts/minute which was determined by observing the counting rate from an un-irradiated crystal.

CALCULATION OF CROSS SECTIONS

After determining the activity of the samples it was necessary to perform various calculations to relate these activities to an absolute cross section. The formulas used in this calculation are given in detail

Fig. 9 - Pulse height distribution of Na^{24} activity.

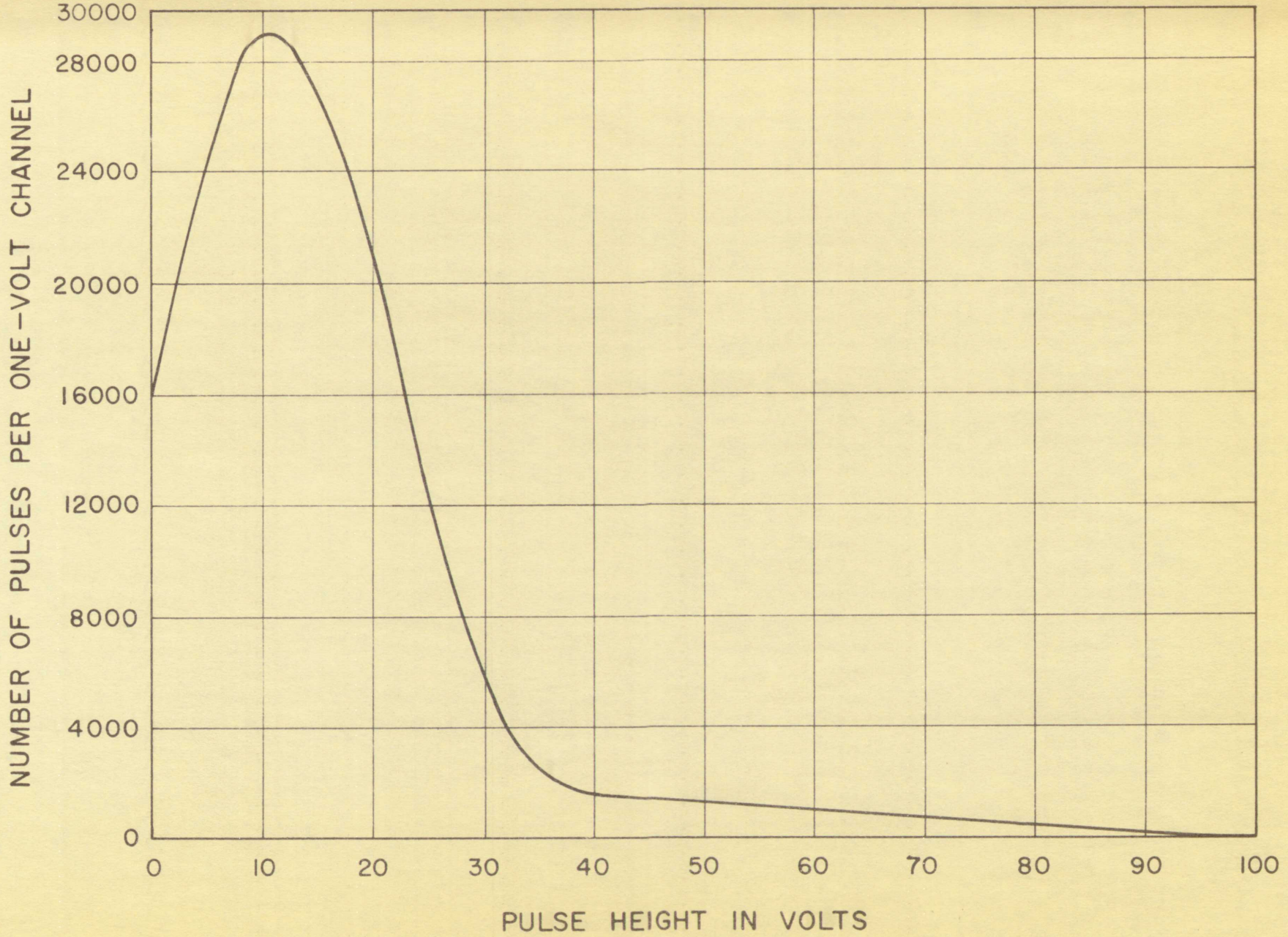
30000
28000
24000
20000
16000
12000
8000
4000
0
NUMBER OF PULSES PER ONE-VOLT CHANNEL
0
10
20
30
40
50
60
70
80
90
100
PULSE HEIGHT IN VOLTS

below.

The time rate of change of the number of radioactive nuclei with a constant rate of production is given by the following differential equation:

$$dP/dt = -\lambda P(t) + R$$

dP/dt = rate of change of number of radioactive nuclei at time t during the irradiation.

λ = decay constant of the radioactive nuclei.

$P(t)$ = number of radioactive nuclei present at time t during the irradiation.

R = rate of production of the radioactive nuclei.

The expression used for the rate of production of the radioactive nuclei by neutrons of energy E_n was:

$$R(E_n) = \sigma_{n,\gamma}(E_n)\, nF(t)\, \Omega$$

$R(E_n)$ = rate of production of radioactive nuclei.

$\sigma_{n,\gamma}(E_n)$ = (n,γ) cross-section of the target nuclei at the neutron energy E_n.

n = number of target atoms per cm^2 in the target.

$F(t)$ = number of neutrons of energy E_n per unit solid angle per second.

Ω = solid angle subtended by the target from the source.

Integration of the above differential equation gives the following expression for $P(t)$:

$$P(t) = R(E_n)\left[1 - e^{-\lambda t}\right]/\lambda$$

However, for irradiation times short compared with the half-life of the activity, as was the case for most of the I^{127} and Na^{23} irradiations, a simplifying approximation was made. It was assumed that the total number of radioactive atoms, N_o, produced in the sample was created instantaneously

at the midpoint of the irradiation interval and subsequently decayed, with no further production, from that time. The expression for N_o is

$$N_o = \sigma_{n,\gamma}(E_n)\, n\Omega \int F(t)dt$$

In this expression $\int F(t)dt$ is the total number of neutrons per unit solid angle during the irradiation interval. The assumption results in less than 0.1% error for both the I^{127} and Na^{23} cases since the irradiation periods were about 1/8 of the half lives.

For the 11 hour Na^{23} irradiation, the number of counts from the long counter was recorded every half-hour and the total activity produced during each half-hour period was assumed to be made at the midpoint of the period. The total number of Na^{24} atoms, N_o, present at the time of no further production was given by the following expression:

$$N_o = \sigma_{n,\gamma}(E_n) n\Omega \sum_{i=1}^{m} \left[e^{-\lambda t_i} \int_i F(t)dt \right]$$

t_i = interval of time from the midpoint time of the i^{th} irradiation period until the time of no further production.

m = total number of irradiation intervals.

The activity after no further production will decay by the well-known law of radioactivity decay

$$N = N_o\, e^{-\lambda t}$$

N = number of radioactive atoms remaining after a length of time t.

N_o = number of radioactive atoms at the end of the irradiation.

The iodine activity was counted in the following manner. The integrated number of pulses I (with background subtracted) was obtained in the multichannel analyzer in the time interval t_1 to t_2. The number of

counts was related to N_o in the following manner:

$$I = N_o\left[e^{-\lambda t_1} - e^{-\lambda t_2}\right]$$

for which

$$\sigma_{n,\gamma}(E_n) = I/\Omega n\int F(t)dt\left[e^{-\lambda t_1} - e^{-\lambda t_2}\right]$$

In the case of the sodium activities, the counting times necessary to obtain good counting statistics were short compared with the half-life of the activity. The integrated number of counts from the multichannel analyzer was divided by the counting interval time to give a decay rate which was taken to be for the midpoint time of the counting interval. This approximation resulted in an error of less than 0.1% which is negligible compared with other errors in the experiment. The decay rate was related to the original number of radioactive atoms N_o by

$$-dN/dt = \lambda N_o e^{-\lambda t}$$

The integrated neutron flux per unit solid angle $\int F(t)dt$ was determined in the manner described in the section, Measurement of Neutron Flux.

The solid angle Ω subtended by the 0.5 cm thick crystals from the lithium target with crystal-to-target distances of 10 cm was calculated by the formula

$$\Omega = 2\Pi(1 - \cos\theta).$$

Ω = solid angle subtended by the crystal.

θ = the angle whose tangent is the radius of the crystal divided by the distance from the center of the crystal to the lithium layer.

The tritium gas target, unlike the lithium target, has a length of 3 cm so that it did not approximate a point source of neutrons. An average solid angle subtended by the crystal from the target was found by integrating the expression given above over the length of the target. Figure 10 shows the crystal-source geometry. The solid angle subtended by the central cross section of the crystal at a distance R from a point in the target is given by

$$\Omega(R) = 2\pi\left[X^2/2\ (1 - \tfrac{3}{4} X^2)\right]$$

X = radius of crystal/R.

This expression comes from the series expansion of cosθ and is good to 0.1% or better for X less than 0.2. Assuming a constant yield of neutrons throughout the target an average solid angle $\overline{\Omega}$ was obtained from the following expression:

$$\overline{\Omega} = \int_{L}^{L+t} \Omega(R)dR \Big/ \int_{L}^{L+t} dR$$

In the case of the 1 cm thick crystals, which were used at close distances for most of the Na irradiations, the same type of analysis was used to average the solid angle over the length of the crystal as well as the target. For irradiations made with the 0.5 cm thick crystals, the source to crystal separation was large enough that it was not necessary to average the solid angle over the crystal length.

Since a crystal subtended a finite solid angle from the neutron source, a diverging beam of neutrons was incident on the crystal. The average path length of the neutrons in the crystal was somewhat longer than the thickness of the crystal. In order to account for this effect, the cross sections

Fig. 10 - Crystal-source geometry for a finite-length target.

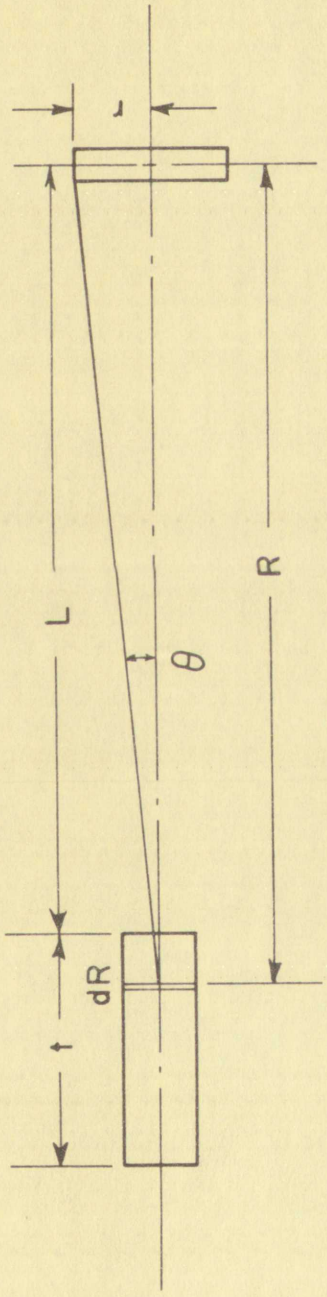
l
L
R
θ
dR
t

were decreased by a factor of $1/\cos\theta$, where θ was the average angle of incidence of the neutrons on the crystal. In the case of the sodium, the cross sections were reduced by 1.5%, while for iodine, the corrections were negligibly small.

Assuming a constant scattering cross section of 10 barns for a NaI molecule over the neutron energy range covered,[3] calculations show that about 15% of the incident neutrons are scattered in the crystal. Approximate calculations indicate that the effect of these scattered neutrons is to increase the path length of the neutrons in the crystal by about 3%. Thus, the cross sections were reduced by a factor of 3%. A probable error of ± 2% was assigned to the measurement because the scattering cross section is not known exactly and also because the calculations were only approximate.

The effects of the thermal neutron flux which arise from room scattering, air scattering, etc., must be considered since the (n,γ) cross sections at thermal neutron energies are quite high, about 90 barns for iodine and 0.56 barns for sodium. The effect was determined in the case of iodine by irradiating a crystal covered with 0.016 inch cadmium sheet and comparing the resulting activity with the activity produced in a crystal without cadmium covering. No difference in the two activities, within counting statistics was observed.

RESULTS

Tables I and II show the (n,γ) cross sections obtained for the $I^{127}(n,\gamma)I^{128}$ and $Na^{23}(n,\gamma)Na^{24}$ reactions along with the U^{235} fission cross sections that were used in the calculations of the absolute values of the (n,γ) cross sections. The neutron energy spread for each neutron energy is also given in the tables. The errors in the cross sections are estimated to be about ± 30% for neutron energies below 60 kev, about ± 12% for neutron energies between 60 kev and 150 kev and about ± 8% for neutron energies above 150 kev.

Table III shows the estimated probable error for the various quantities used in determining the absolute (n,γ) cross sections and further shows the manner in which the errors were compounded. Table III also shows that the uncertainty in the absolute value of the U^{235} fission cross section is the limiting factor in establishing an absolute scale for the (n,γ) cross sections. If more accurate values for the fission cross section of U^{235} becomes available in the future, the (n,γ) cross sections for iodine and sodium presented here can be corrected accordingly.

Figure 11 shows a log-log plot of the (n,γ) cross sections for iodine versus neutron energy. No resonances in the curve are evident in this neutron energy range. This result would be expected because the energy level spacing in a medium weight nucleus such as iodine is closer than the energy resolution of the experiment. By simple theory, in the energy region below 1 kev, (n,γ) cross sections should roughly follow a $1/v$ law where v is the velocity of the neutron. At higher neutron energies the cross sections should follow a $1/v^2$ expression. The cross section curve for iodine decreases more rapidly than $1/v$ in the energy range up to 100 kev and above 100 kev decreases even more rapidly but not as rapidly as $1/v^2$. The cross sections are relatively large, ranging from 1 barn at 25 kev to 80 mb at 1 Mev; thus iodine lends itself particularly well as a secondary standard for the measurement of neutron fluxes.

Figure 12 shows a log-log plot of the (n,γ) cross sections for sodium versus neutron energy. Several peaks are observed in this neutron energy range. Sodium is a light weight nucleus and the energy level spacing is quite wide compared with the level spacing in iodine, so it might be expected that resonance structure would appear in the excitation curve. The

TABLE I. Cross sections for $I^{127}(n,\gamma)I^{128}$ reaction.

E_n kev	$\sigma_{n,\gamma}$ mb	ENERGY SPREAD High E_n	ENERGY SPREAD Low E_n	σ_f b
19	1100	24	13	3.13
42	760	46	39	2.46
59	560	65	53	2.21
78	436	82	75	2.01
103	409	110	97	1.84
131	350	139	122	1.70
155	317	163	147	1.62
178	265	185	170	1.56
187	270	200	175	1.54
203	249	216	191	1.50
209	226	216	202	1.50
218	233	230	206	1.48
222	254	229	215	1.48
233	219	245	221	1.46
238	200	245	231	1.46
246	208	258	235	1.44
260	202	272	249	1.43
265	204	272	258	1.42
274	194	286	263	1.41
288	185	300	277	1.39
291	195	298	285	1.39
302	169	314	291	1.37
319	178	325	313	1.36
345	164	352	339	1.34
372	167	378	366	1.32
397	159	404	389	1.29
422	148	429	415	1.27
447	142	455	440	1.26
472	129	479	465	1.24
497	126	505	490	1.23
523	131	530	516	1.23
548	126	555	541	1.22
471	132	527	415	1.25
554	130	608	500	1.22
656	115	708	603	1.19
759	95	809	708	1.18
857	86	905	808	1.18
985	80	1033	937	1.27

TABLE II. Cross sections for the $Na^{23}(n,\gamma)Na^{24}$ reaction.

E_n kev	$\sigma_{n,\gamma}$ mb	ENERGY SPREAD High E_n	ENERGY SPREAD Low E_n	σ_f b
30	3.00	43	18	2.70
40	2.57	58	25	2.50
55	2.23	80	36	2.26
80	1.09	110	54	2.00
112	1.46	148	80	1.78
171	0.83	210	135	1.57
183	0.92	229	137	1.55
242	0.73	285	200	1.45
299	0.73	339	259	1.38
352	0.40	391	313	1.33
404	0.29	443	366	1.29
456	0.25	494	418	1.26
508	0.30	541	476	1.23
562	0.33	644	480	1.22
662	0.35	743	581	1.19
768	0.29	842	694	1.18
865	0.16	936	793	1.18
996	0.22	1064	927	1.27

TABLE III. Probable errors assigned to quantities used in determining the absolute (n,γ) cross sections.

Source of error	Percentage Probable Error (e)		
	Neutron Energies above 150 kev	Neutron Energies between 60 kev and 150 kev	Neutron Energies below 60 kev
U^{235} fission cross section	5	10	30
Neutron scattering into long counter by fission detector	2	2	2
Neutron scattering in the fission detector	2	2	2
Counting statistics of fission detector	3	3	3
Integration of fission distribution to determine fission events	2	2	2
Geometry (measurements of distances and angles)	3	3	3
Neutron scattering in the crystal	2	2	2
Determination of the induced activity of the crystals	2	2	2
Total $=\sqrt{\sum e^2}$	±8%	±12%	±30%

Fig. 11 - Absolute excitation function for the $I^{127}(n,\gamma)I^{128}$ reaction.

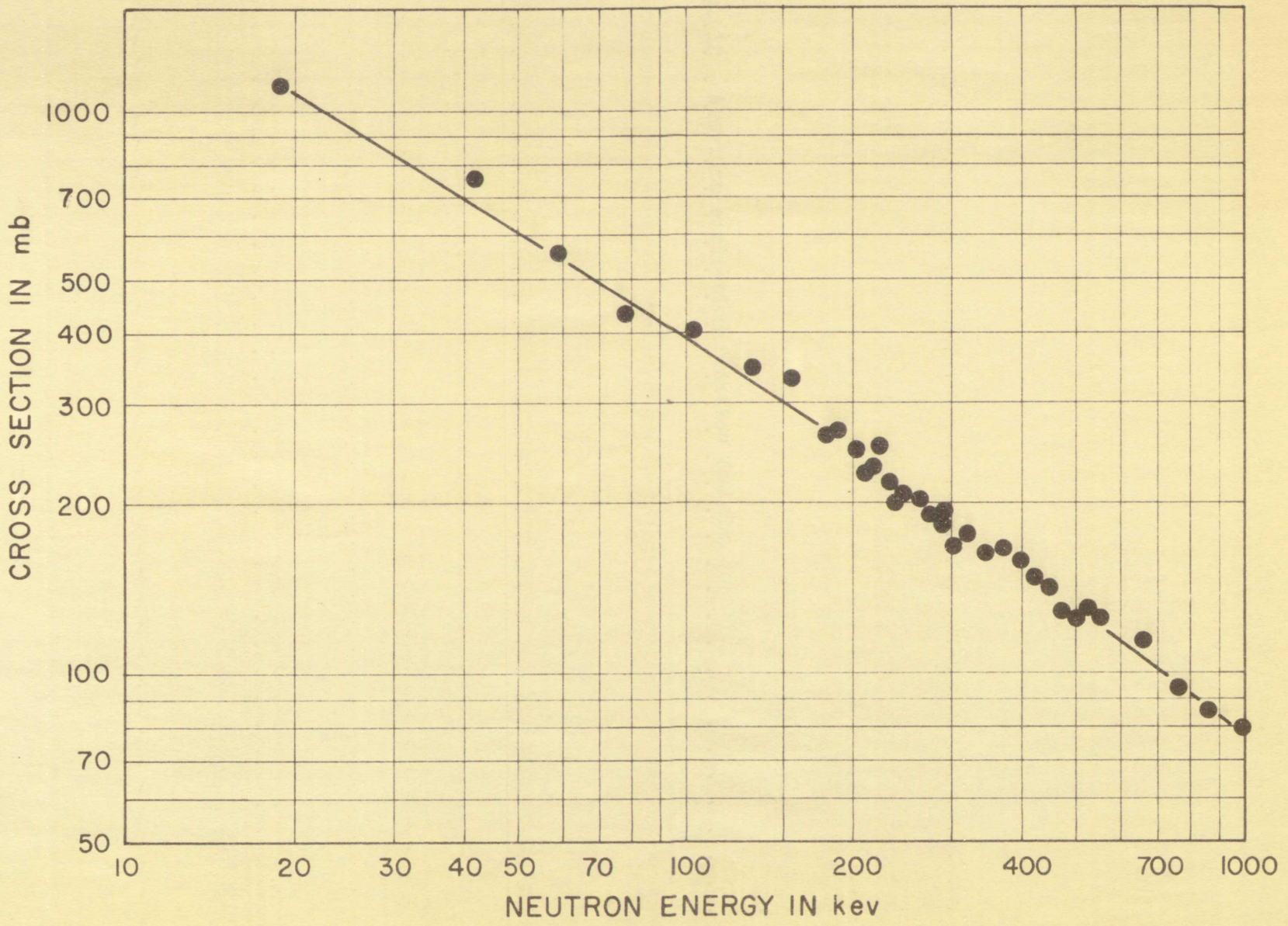
CROSS SECTION IN mb
1000
700
500
400
300
200
100
70
50
10
20
30
40
50
70
100
200
400
700
1000
NEUTRON ENERGY IN kev

Fig. 12 - Absolute excitation function for the $Na^{23}(n,\gamma)Na^{24}$ reaction.

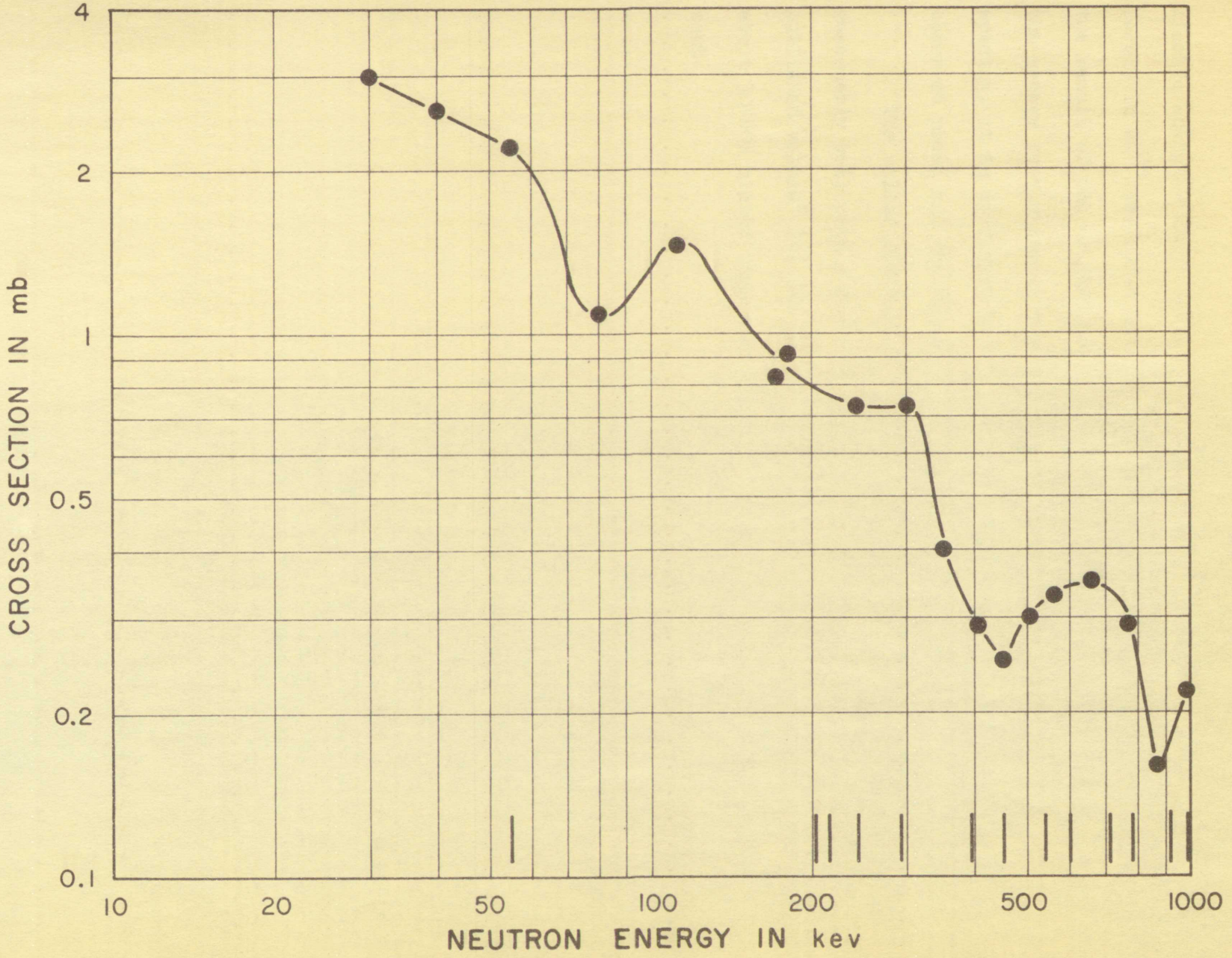
4
2
1
0.5
0.2
0.1
CROSS SECTION IN mb
10
20
50
100
200
500
1000
NEUTRON ENERGY IN kev

kinetic energies which neutrons must have in order to excite known energy levels in Na^{24} are shown in Fig. 12. The peak at about 120 kev might be the result of one or more not yet discovered energy levels in Na^{24}. Since the energy resolution of the experiment is large compared to the level spacing, it is difficult to make more than a rough correspondence between the observed peaks and the known energy levels.

The values obtained for the (n,γ) cross sections for sodium agree reasonably well with a few isolated values that have been published.[3] The published values[3] for the (n,γ) cross section for iodine are systematically about 50-60% higher than the corresponding values obtained in this experiment.

LIST OF REFERENCES

[1] E. Segre, Experimental Nuclear Physics, John Wiley and Sons (1953), II, pp. 321-325.

[2] J. Hollander, I. Perlman, and G. Seaborg, Rev. Mod. Phys. 25, 469 (1953); also N. Benczer and others, Phys. Rev. 101, 1027 (1956).

[3] D. Hughes and R. Schwartz, Neutron Cross Sections, Brookhaven National Laboratory (1957) Supplement I to BNL 325.

[4] R. F. Taschek and A. Hemmendinger, Phys. Rev. 74, 373 (1948); A. Langsdorf, J. Monahan and W. A. Reardon, A Tabulation of Neutron Energies from Monoergic Protons on Lithium, Argonne National Laboratory, 5219 (1954).

[5] A. O. Hanson and J. L. McKibben, Phys. Rev. 72, 673 (1947).

[6] G. Jarvis and others, Phys. Rev. 79, 929 (1950); J. Marion and B. Allen, A Tabulation of Neutron Energies from Various Charged Particle Reactions, Shell Development Company, (1955).

[7] J. L. Fowler and J. E. Brolley, Phys. Rev. 28, 103 (1956).

[8] D. W. Allen and R. L. Henkel, Progress in Nuclear Engineering (Pergamon Press), Series I, II (in press).

[9] H. A. Bethe, J. R. Beyster and R. E. Carter, Journal of Nuclear Energy, 4, 3 (1957).